Mechanical and Thermal Properties of Hot-Pressed ZrB$_2$-SiC Composites

SHIRSHENDU CHAKRABORTY, DEBASHISH DEBNATH,
AZIZUR RAHAMAN MALLICK, and PROBAL KUMAR DAS

ZrB$_2$-SiC composites were hot pressed at 2473 K (2200 °C) with graded amounts (5 to 20 wt pct) of SiC and the effect of the SiC addition on mechanical properties like hardness, fracture toughness, scratch and wear resistances, and thermal conductivity were studied. Addition of submicron-sized SiC particles in ZrB$_2$ matrices enhanced mechanical properties like hardness (15.6 to 19.1 GPa at 1 kgf), fracture toughness (2 to 3.6 MPa(m)$^{1/2}$) by second phase dispersion toughening mechanism, and also improved scratch and wear resistances. Thermal conductivity of ZrB$_2$-SiC (5 wt pct) composite was higher [121 to 93 W/m K from 373 K to 1273 K (100 °C to 1000 °C)] and decreased slowly upto 1273 K (1000 °C) in comparison to monolithic ZrB$_2$ providing better resistance to thermal fluctuation of the composite and improved service life in UHTC applications. At higher loading of SiC (15 wt pct and above), increased thermal barrier at the grain boundaries probably reduced the thermal conductivity of the composite.

I. INTRODUCTION

STRUCTURAL ceramics for use in ultra high temperature environments are presently focused on Zr- and Hf-borides, carbides and nitrides because of their high melting point, high hardness and fracture toughness, high thermal conductivity and good thermal shock resistance, and chemical stability in severe condition.[1–5] In particular, many researchers recommended use of monolithic ZrB$_2$ over carbides and nitrides of Zr and Hf because of its lower cost and lighter weight (theoretical density of ZrB$_2$ = 6.09 gm/cc) that makes it a potential and promising material for structural, aerospace, and other conventional fields like refractory crucible, electrode, thermal plant etc[6–9] However, the use of monolithic ZrB$_2$ for real time UHTC applications is limited because of its relatively low hardness and fracture toughness and poor oxidation resistance specially above 1273 K (1000 °C) than its composites. ZrB$_2$ is also very difficult to sinter because of its strong covalent nature, low diffusion rates, and the presence of oxygen on the particle surfaces.[10,11] More work is in progress for further reduction of weight of ZrB$_2$ system without compromising other desired structural properties to meet the future demands of strategic sectors and thermal protection units.[12] Toward this goal, fabrications of ZrB$_2$ composites are being investigated by the researchers to retain and/or improve the mechanical and thermal properties. Various approaches include the addition of secondary phases ($e.g.$, SiC, Carbon, MoSi$_2$, ZrC, WC, B$_4$C, $etc.$) and sintering aids, changing precursor material characteristics, processing parameters like temperature, pressure, and processing techniques $viz.$, spark plasma sintering, hot pressing, hot isostatic pressing, self-propagating high-temperature synthesis (SHS), pressure-less sintering, microwave sintering, laser sintering, $etc.$[1,13–22] Moreover, machining and frictional behavior need to be evaluated to ascertain the performance of a structural UHTC component like ZrB$_2$-SiC composite.[23] However, studies on tribological properties that include coefficient of friction, wear resistance, and wear rate under different load of ZrB$_2$-SiC composites are scarce. Therefore, it is necessary to study the tribological behavior of ZrB$_2$-SiC composites for fabrication of next generation UHTC components.

In present study, the effect of the SiC loading on mechanical properties like hardness, fracture toughness, scratch resistance, wear resistance and thermal conductivity of a series of hot pressed ZrB$_2$-SiC composites was investigated and compared to those of monolithic ZrB$_2$ ceramic.

II. EXPERIMENTAL

A. Materials

In the present work, phase pure zirconium diboride (ZrB$_2$-B Grade) and silicon carbide (SiC-UF25 Grade) powders were procured from H.C Starck GmbH, Goslar, Germany, as raw materials. As per technical data provided by H.C Starck, oxygen content of ZrB$_2$ powder is 1.5 wt pct, and other impurities are carbon 0.2, nitrogen 0.25, Fe 0.1, and Hf 0.2, and in SiC

SHIRSHENDU CHAKRABORTY, Scientist, DEBASHISH DEBNATH, Project Assistant, AZIZUR RAHAMAN MALLICK, Project Fellow, and PROBAL KUMAR DAS, Chief Scientist, are with the Non Oxide Ceramics and Composites Division, CSIR-CGCRI, 196 Raja S C Mullick Road, Kolkata 700032, WB, India. Contact e-mail: shirshenduc@yahoo.com, shirshendu@cgcri.res.in

powder impurities are oxygen 2.5, Al 0.04, Ca 0.01, and Fe 0.05 (in wt pct). ZrB_2 and SiC powders are of particle size (D_{50}) 3.22 and 0.45 μm, respectively. ZrB_2-SiC mixed powders containing 5, 10, 15, and 20 wt pct SiC were prepared. The stoichiometric amount of component powders in each batch, *i.e.*, ZrB_2 with 5 to 20 wt pct SiC was mixed in a mortar pestle in methyl ethyl ketone medium for 1 hour each and then dried at 80 °C in an oven.

B. Hot Pressing

Mixed batch powders were hot pressed at 2473 K (2200 °C) in argon atmosphere in a graphite element hot press (HPW 315/400-2200-1000PS, FCT Systeme GmbH, Germany) under a pressure of 50 MPa and soaking time of 2 hour. To minimize reaction between graphite die and precursor powders, inner wall of graphite dies was lined with thin graphite paper (0.25 mm thick) before powder was loaded. The heating and cooling rates of the furnace were kept in the range of 15 to 25 °C/min. Diameter and thickness of the sintered compacts were around 75 and 6 mm, respectively.

C. Characterization

The sintered samples were ground on both sides and sliced into small pieces by precision surface grinder (NKT6, ELB-Scliff, Germany) fitted with diamond grinding wheel and saw. Bulk density (and pct of relative density) of the sintered samples was measured by Archimedes' principle. The theoretical density of each composite was calculated by the mixture rule. The phase investigation of samples was done by X-ray powder diffraction technique (X'Pert Pro MPD; Pan-Analytical, The Netherlands) with CuK_α radiation (α = 1.54 Å) at room temperature. The XRD data were recorded with step size 0.05 deg (2θ) and step time 75 seconds from 20 to 90 deg for these samples. The microstructure and also the elemental analysis (EDS) of the ZrB_2-SiC composites were done by Field Emission Scanning Electron Microscope (FESEM) (AXIOS; Pan-Analytical, The Netherlands). Micro-hardness tests at different loads (500 gmf and 1 kgf) were carried out using Vickers Micro-hardness tester (402MVD, Wolpert Wilson) with a 10 seconds dwell time and the indentation photographs were taken automatically by attached the CCD camera (FM290223, Precidur). The reported data are an average of four hardness measurements. Fracture toughness values were calculated by direct crack method (DCM). Scratch test was conducted using a Scratch tester (TR-101, Ducom, India) at room temperature (dry and un-lubricated conditions) at a relative humidity level of 60 ± 5 pct. A Vickers type diamond tip was used as a sliding contact on the vibration free samples to measure the coefficient of friction at two different normal loads (5 and 10 N). Indenter velocity was kept fixed at 0.1 mm/s, and the length of sliding was set in all cases 4 mm. The samples for both hardness and scratch tests were mounted in resin and polished by a surface polisher (Spectrum System 1000, LECO Corporation) to achieve uniform surface roughness (R_a) in the range of 50 to 70 nm as shown in Figure 1. The surface roughness of the specimen was measure by non-contact type profilometer (Contour GT-X, Bruker Corporation). Thermal conductivity of the composites was measured by laser flash technique (Flash Line 4010, Anter Corporation). The instrument can automatically determine thermal conductivity, heat capacity, and thermal diffusivity. In thermal measurement, 10 ± 0.5 mm square specimens with carbon coating were used.

III. RESULTS AND DISCUSSION

A. Densification

The relative and bulk density of hot-pressed ZrB_2 and SiC monolithics and ZrB_2-SiC composites are shown in Figure 2. Relative density of the ZrB_2-SiC composites decreases with higher amount of SiC addition (above 5 wt pct). The oxygen impurities of SiC power are higher than ZrB_2. Higher amount of surface oxygen in SiC particles (depleted amount of surface oxygen) may act as boundary phase at higher SiC loading that hinder the lattice diffusion and hence, restrict the sintering of
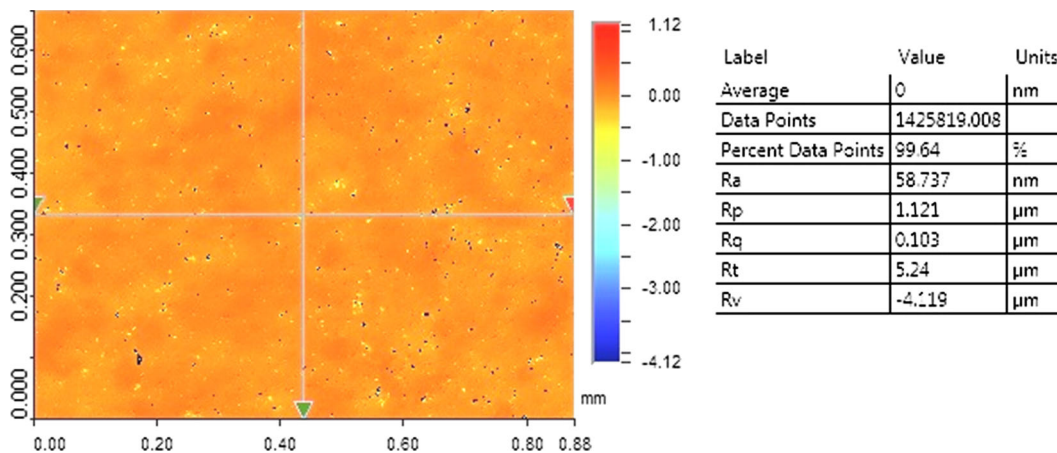

Label	Value	Units
Average	0	nm
Data Points	1425819.008	
Percent Data Points	99.64	¾
Ra	58.737	nm
Rp	1.121	µm
Rq	0.103	µm
Rt	5.24	µm
Rv	-4.119	µm

Fig. 1—2D surface topography of polished ZrB_2-SiC composite.

ZrB$_2$-SiC composites.[24,25] At high temperature consolidation, residual pores are mainly formed as closed porosity, and reduction of porosity is governed by grain boundary diffusion. The presence of submicron-sized SiC grains in the ZrB$_2$ matrix prevents grain boundary movement and hinder coarsening. M. Ikegami reported that relative densities exceeding 98 pct were found for ZrB$_2$-SiC (10 to 30 vol pct) composites by spark plasma sinrering at 2173 K (1900 °C) under 30 MPa. The formation of intergranular liquid phase at grain boundaries played a key role for achieving high densifica-

tion.[26] Asl showed that the sintering of hot-pressed ZrB$_2$-SiC (15 and 30 vol pct) composite at 2273 K (2000 °C) mainly controlled by grain boundary diffusion, whereas plastic deformation dominated densification for monolithic ZrB$_2$ at relatively lower temperature *i.e.*, 2123 K (1850 °C).[27] Hence, cumulative effects of coarsening, evaporation/condensation, grain boundary, and lattice diffusion processes are governing densification mechanism.

B. *XRD Study*

Figures 3(a) through (d) show the XRD plots of ZrB$_2$-SiC composites sintered at 2473 K (2200 °C) for 2 hour. JCPDS files (a) 75 to 1050 & (b) 75 to 1541 reveal that both hexagonal ZrB$_2$ and hexagonal α-SiC phases are distinctly present in all samples. The crystallite sizes of ZrB$_2$ and SiC particles in ZrB$_2$-SiC composites calculated to be in the range of 60 to 90 nm from the X-ray diffraction patterns (Figures 3(a) through (d)) using Scherrer formula:

$$D = 0.9\lambda/\beta\cos\theta, \qquad [1]$$

where D is the average crystallite size, $\lambda = 1.54$ Å [X-ray wavelength (CuKα)], and β being the width of the diffraction peak at half maximum for the diffraction angle 2θ.

C. *Microstructure*

Figures 4(a) through (d) show the FESEM microstructure images of monolithic ZrB$_2$ and ZrB$_2$-SiC
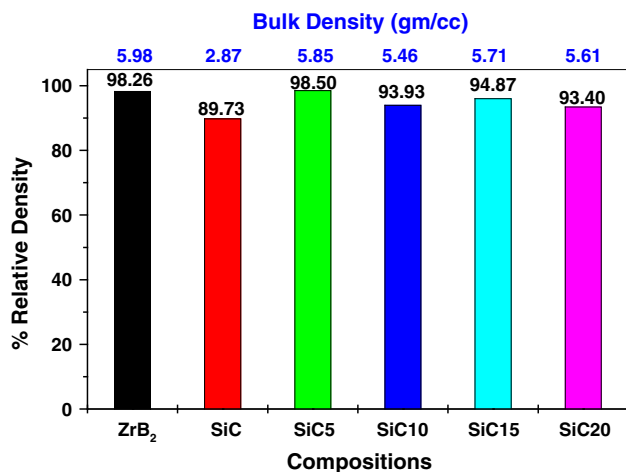
Fig. 2—Bulk density and pct relative density of ZrB$_2$-SiC composites hot pressed at 2473 K (2200 °C) for 2 h (Notation: SiC 5 = ZrB$_2$ + SiC (5 wt pct) and others are equivalent).
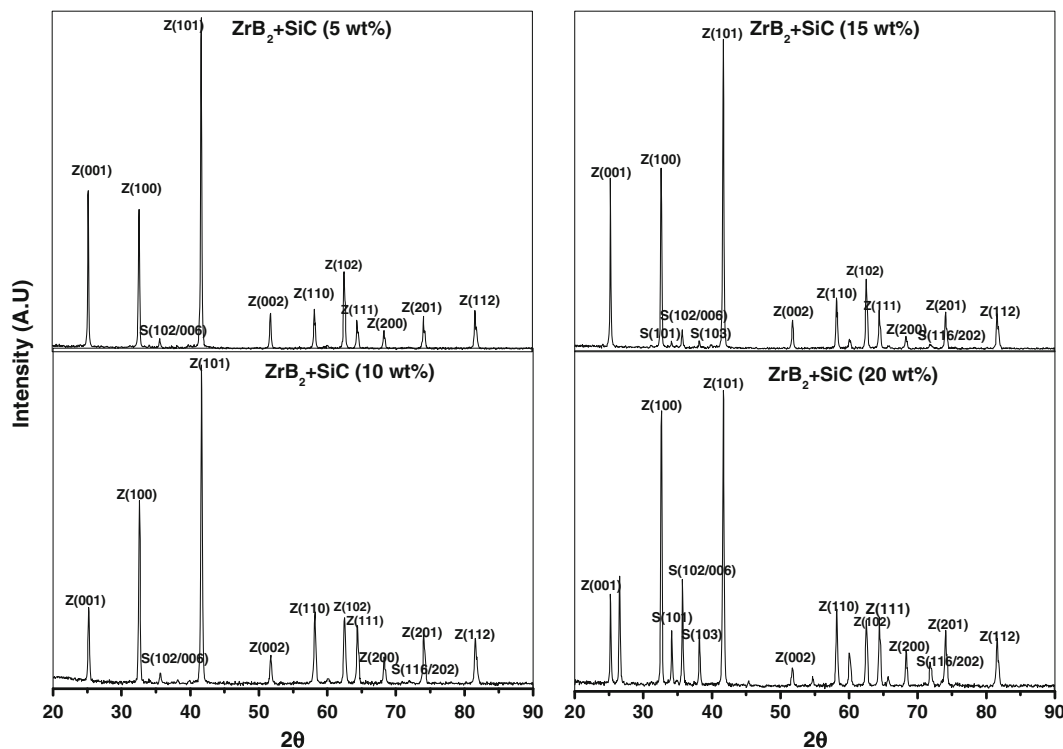
Fig. 3—XRD plots of ZrB$_2$-SiC composites hot pressed at 2473 K (2200 °C) for 2 h soaking (*a*) ZrB$_2$-SiC (5 wt pct), (*b*) ZrB$_2$-SiC (10 wt pct), (*c*) ZrB$_2$-SiC (15 wt pct), and (*d*) ZrB$_2$-SiC (20 wt pct) (notation Z = ZrB$_2$, S = α-SiC).
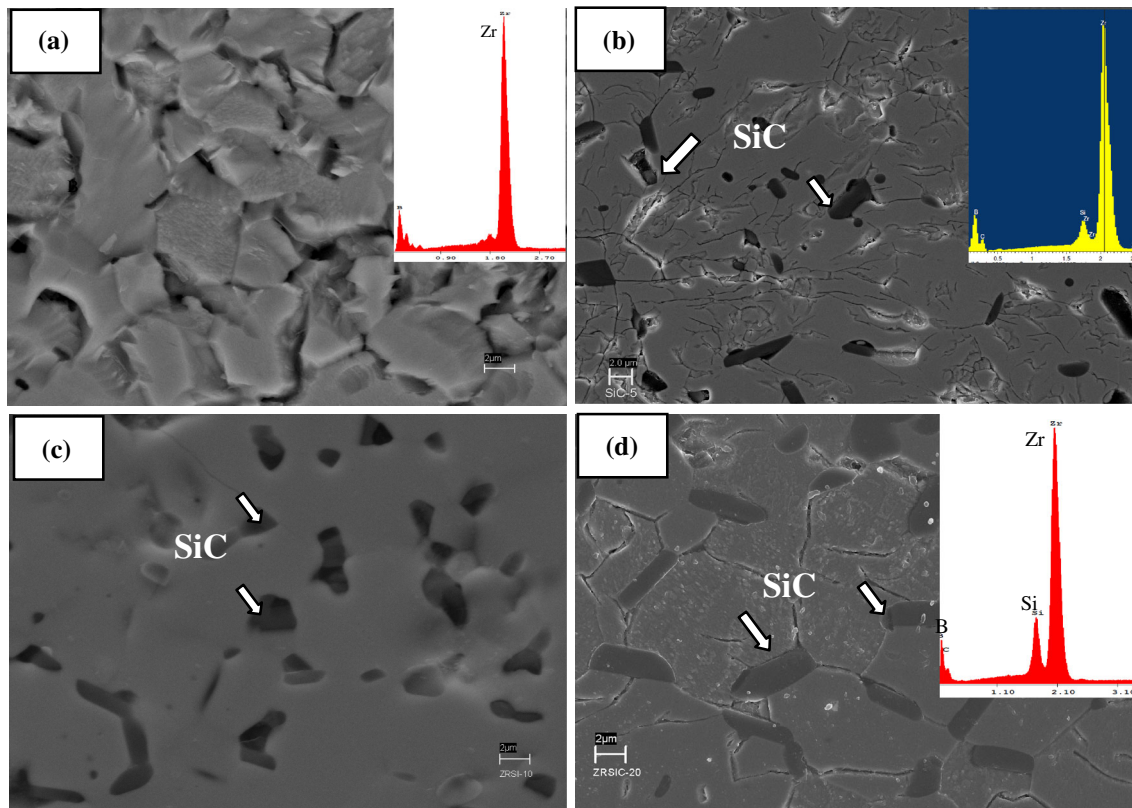
Fig. 4—FESEM microstructure and EDS mapping of (a) monolithic ZrB_2, (b) ZrB_2-SiC (5 wt pct), (c) ZrB_2-SiC (10 wt pct), and (d) ZrB_2-SiC (20 wt pct) composites hot pressed at 2473 K (2200 °C)/2 h (bright phase is ZrB_2 and dark phase is SiC).

composites hot pressed at 2473 K (2200 °C) for 2 hour after polishing and finally etching with diluted hydrofluoric acid. It is clearly stated from the micrographs (Figures 4(b) through (d)) that SiC grains (dark phase) are uniformly distributed in ZrB_2 matrix (bright phase) that can macroscopically interpret the mechanical strength of the composite. Elemental analysis by EDS spectra also confirms that only Zr, Si, B, and C elements composed of ZrB_2 and SiC phases are present in the microstructures and support the above XRD results.

D. Mechanical and Tribological Properties Study

Vickers micro-hardness and fracture toughness data of hot-pressed ZrB_2 and SiC monolithics and ZrB_2-SiC composites at different loads (500 gms and 1 kgs) are summarized in Table I. 'Anstis' employed a simplified two-dimensional fracture mechanics analysis by DCM[28]:

$$K_{IC} = 0.016 \, (E/H)^{1/2} \times F/C^{3/2}, \qquad [2]$$

where F is load in Newton; C is crack length from the center of the indent to the crack tip in meter; E is Young's modulus in GPa calculated by the rule-of-mixture model ($E_{ZrB2} = 520$ GPa, $E_{SiC} = 400$ GPa); H is Vickers hardness in GPa; and K_{IC} is fracture toughness in MPa(m)$^{1/2}$.

This classification is applicable for cracks in brittle ceramic materials with relatively low toughness and considered to follow half-penny model, where the crack length is measured radially from the center of the indentation. It is observed that all samples exhibit an increase in the hardness with decreasing indentation load (indentation size effect; ISE) that mainly arises due to elastic recovery of the indentation after removal of indenter load and is proportionately more prominent in small indentation and also results in changing dislocation density of coarse grain bulk materials.[29] Indentation and micro-cracks profile (inset) are shown in Figure 5. Fracture toughness values of monolithic ZrB_2 and SiC systems are considerably low due to their brittle nature, and it is found from Figure 5(a) that a clear broad radial crack occurs at the corner of the residual impression at the indentation of monolithic ZrB_2, and on the other side in Figure 5(b), slight cracks deflection occurs in ZrB_2-SiC composite which leads to mixed inter-transgranular fracture mode. In case of fracture toughness value of ZrB_2-SiC composite (Table I), it is found that addition of hard SiC material in the ZrB_2 system improves fracture toughness of the composite by toughening mechanisms like crack deflection and stress relaxation near the crack tip after addition of SiC as secondary phase, and all cracks are shallow in nature.[31,32] Liu et al. reported that addition of nanosized SiC ($D_{avg} = 0.7 \, \mu m$) in the ZrB_2 system improved the fracture toughness (6.4 MPa m$^{1/2}$) and flexural strength (925 MPa) than ZrB_2 composite with microsized SiC particles.[33] Guo et al. showed that hot-press ZrB_2-SiC (20 vol pct)-Yb_2O_3 (3 vol pct) compos-

Table I. Vickers Hardness and Fracture Toughness Values of Monolithic ZrB₂ and SiC and ZrB₂-SiC Composites Hot Pressed at 2473 K (2200 °C)/2 h

| Sl No	Composition	Vickers Hardness (GPa)		K_{IC} (MPa(m)$^{1/2}$) [c/a ratio]	
		1 kgf	500 gf	1 kgf	500 gf
1	ZrB₂[30]	14.40 ± 1.33	15.48 ± 1.45	2.52 ± 0.13 [2.43]	2.76 ± 0.11 [2.52]
2	SiC	15.74 ± 1.21	16.07 ± 1.32	1.48 ± 0.23 [2.60]	1.82 ± 0.23 [2.93]
3	ZrB₂ + SiC (5 wt pct)	19.05 ± 1.42	21.97 ± 1.51	3.63 ± 0.25 [2.32]	3.13 ± 0.24 [2.19]
4	ZrB₂ + SiC (10 wt pct)	19.08 ± 1.53	17.06 ± 1.25	2.49 ± 0.25 [2.81]	2.84 ± 0.23 [2.43]
5	ZrB₂ + SiC (15 wt pct)	17.87 ± 1.51	17.18 ± 1.44	2.58 ± 0.23 [2.94]	3.03 ± 0.25 [2.11]
6	ZrB₂ + SiC (20 wt pct)	15.62 ± 1.62	15.81 ± 1.61	1.97 ± 0.26 [3.25]	2.86 ± 0.24 [2.10]
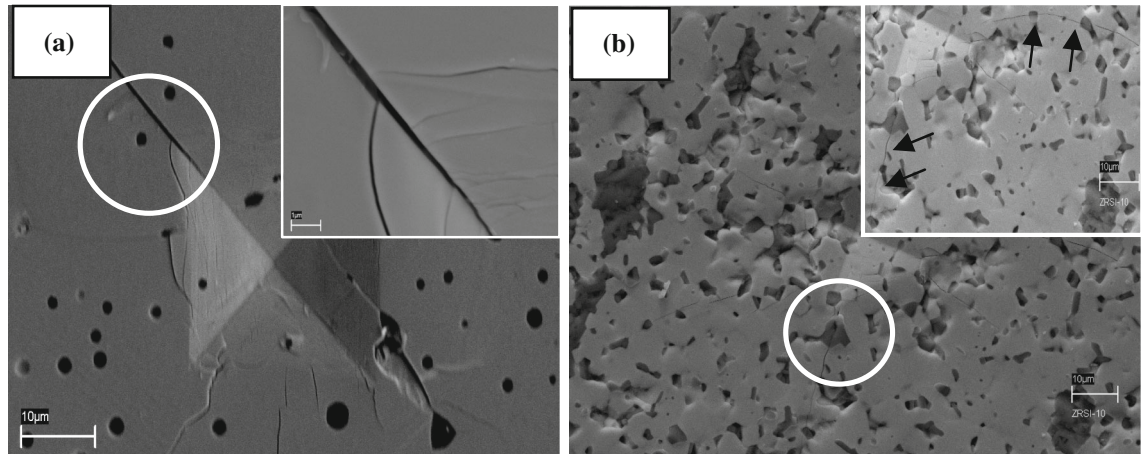
Fig. 5—FESEM images of micro-indentation of (*a*) ZrB₂ monolithic and (*b*) ZrB₂-SiC (10 wt pct) composite (nature of micro-cracks are shown in the insets).

ite achieved high hardness (20.2 GPa) and toughness (4.9 MPa m$^{1/2}$).[34] It is also observed from Table I that the fracture toughness value reduces at higher loading of SiC (20 wt pct). Low sintering density of ZrB₂-SiC (20 wt pct) composite can lower the fracture toughness and hardness values. Anstis *et al.* reported that c/a [*i.e.*, (crack length from the indentation diagonal + half *diameter of indentation*)/half diameter of indentation] is basically assumed to be a proof of the type of crack system.[28] It is stated that if c/a ≥ 2, the crack model is considered as half-penny type or median crack, and if c/a < 2, the crack model is considered as Palmqvist (half-ellipse) model.[35,36] It is found from Table I that all the c/a values are greater than 2 and hence, the cracks are followed to half-penny type model.

It can be seen from Table II that coefficient of kinetic friction (COF, μ_k) values of all the composites lies in the range of 0.49 to 0.72 and clearly seen a initial low-friction (low-wear) region and finally a high-friction (high-wear) region after traveling through a sharp transition region as shown in Figure 6. However, the transition region occurred at a relatively higher sliding distance at high load (10 N). High friction during sliding of indenter generates tensile stresses in the track plane of the sliding surface that initiates cracks and gradually propagates along grain boundaries at very high load that acquires more time to stabilize the COF data at high-friction region. The fluctuations of the COF values

at high-friction region are often due to sliding of the indenter on the hard and polished composite surface, and this behavior is more prominent at high load that required more frictional force to move the stylus into the hard track.

Hardness and wear resistance coefficients were calculated by the standard formuli.[37–39] To calculate the wear volume, a number of 2-D surface profiles across the worn surface were acquired using a non-contact surface profilometer (Contour GT-X, Bruker).

A commonly used equation to calculate the wear rate (or factor) is[40]

$$V_i = k_i \times F \times s, \qquad [3]$$

where F is the normal load on contact, s the sliding distance, V_i the wear volume, and k_i the specific wear rate coefficient. Index i identifies the surface considered. The k-value is given in mm³/Nm.

Both wear resistance coefficient and wear rate values were found to be very low for all composites those are needed for engineering applications (Table III).

E. *Thermal Properties Study*

In hypersonic vehicles, the most significant thermal properties of UHTC materials exhibit thermal conductivity and specific heat that emerge as first-order terms in

Table II.   Coefficient of Friction Values of ZrB$_2$-SiC Composites Hot Pressed at 2473 K (2200 °C)/2 h Under Different Loads

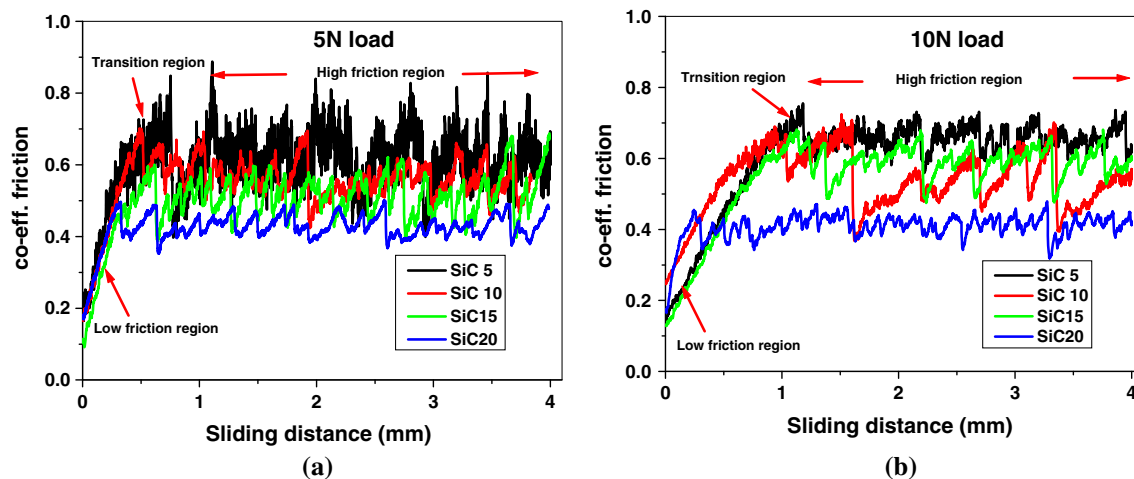|	Coefficient of Friction (μ_k)	
Sample	*5 N*	*10 N*
ZrB$_2$ + SiC (5 wt pct)	0.713	0.723
ZrB$_2$ + SiC (10 wt pct)	0.699	0.691
ZrB$_2$ + SiC (15 wt pct)	0.576	0.681
ZrB$_2$ + SiC (20 wt pct)	0.489	0.552

Fig. 6—Coefficient of friction plots with different loads [(*a*) 5 N and (*b*) 10 N] of ZrB$_2$-SiC composites (Notation: SiC 5 = ZrB$_2$ + SiC (5 wt pct) and others are equivalent).

Table III.   Wear Parameters of ZrB$_2$-SiC Composites Hot Pressed at 2473 K (2200 °C)/2 h Under Different Load

Sample	Fracture Toughness (MPa(m)$^{1/2}$)	Normal Load (N)	Hardness (GPa)	Wear Volume (μm^3)	Wear Resistance Coefficient	Wear Rate (mm^3/Nm)
ZrB$_2$ + SiC (5 wt pct)	3.131	5	21.97	1.872×10^5	0.664	9.36×10^{-3}
	3.650	10	19.05	3.892×10^5	0.443	9.73×10^{-3}
ZrB$_2$ + SiC (10 wt pct)	2.841	5	17.06	0.787×10^5	0.216	3.93×10^{-3}
	2.485	10	16.47	4.767×10^5	0.302	11.92×10^{-3}
ZrB$_2$ + SiC (15 wt pct)	3.525	5	17.18	1.698×10^5	0.625	8.49×10^{-3}
	2.580	10	17.86	6.445×10^5	0.447	16.11×10^{-3}
ZrB$_2$ + SiC (20 wt pct)	3.162	5	15.81	0.861×10^5	0.262	4.31×10^{-3}
	1.965	10	15.62	1.44×10^5	0.065	4.60×10^{-3}

the leading conversion of energy equation. High thermal conductivity allows more heat to conduct away from sharp leading edges and specific heat can have a potential influence on the transient thermal response during heating or cooling. On the other hand, thermal diffusivity (α) of a composite elucidates in combination of electronic and phonon contributions and depends on compositions, porosity, dislocation, cracks, impurities, contact resistance between grains, grain size, sintering schedule *etc*.[41,42] It is seen from Figure 7 that ZrB$_2$-SiC (5 wt pct) composite shows higher thermal conductivity than monolithic ZrB$_2$ and occurs due to the high sintered density of ZrB$_2$-SiC (5 wt pct) composite that improves by reducing interfacial thermal resistance, ensuing in high thermal conductivity.[43–46] It is also observed that thermal conductivity and diffusivity of

ZrB$_2$-SiC composites decrease slowly with increasing temperature than monolithic ZrB$_2$ that means the thermal properties of ZrB$_2$-SiC composites are relatively more stable above 873 K (600 °C). It is reported that the Debye temperature for ZrB$_2$ and SiC are 750 K and 1080 K (447 °C and 807 °C), respectively,[47,48] and electron contribution is more prominent for monolithic ZrB$_2$, whereas addition of SiC increases the phonon contribution in the composite.[49] Therefore, the phonon contribution for thermal conductivity kept constant upto Debye temperature that gives more stable thermal parameters of ZrB$_2$-SiC composite than monolithic ZrB$_2$. M. Patel *et al*. reported that hot-pressed ZrB$_2$-B$_4$C (1 wt pct)-SiC (10 to 30 wt pct) composites showed high thermal conductivity in the range of 85 to 92 W/m.K.[50] Kim *et al*. showed that addition of
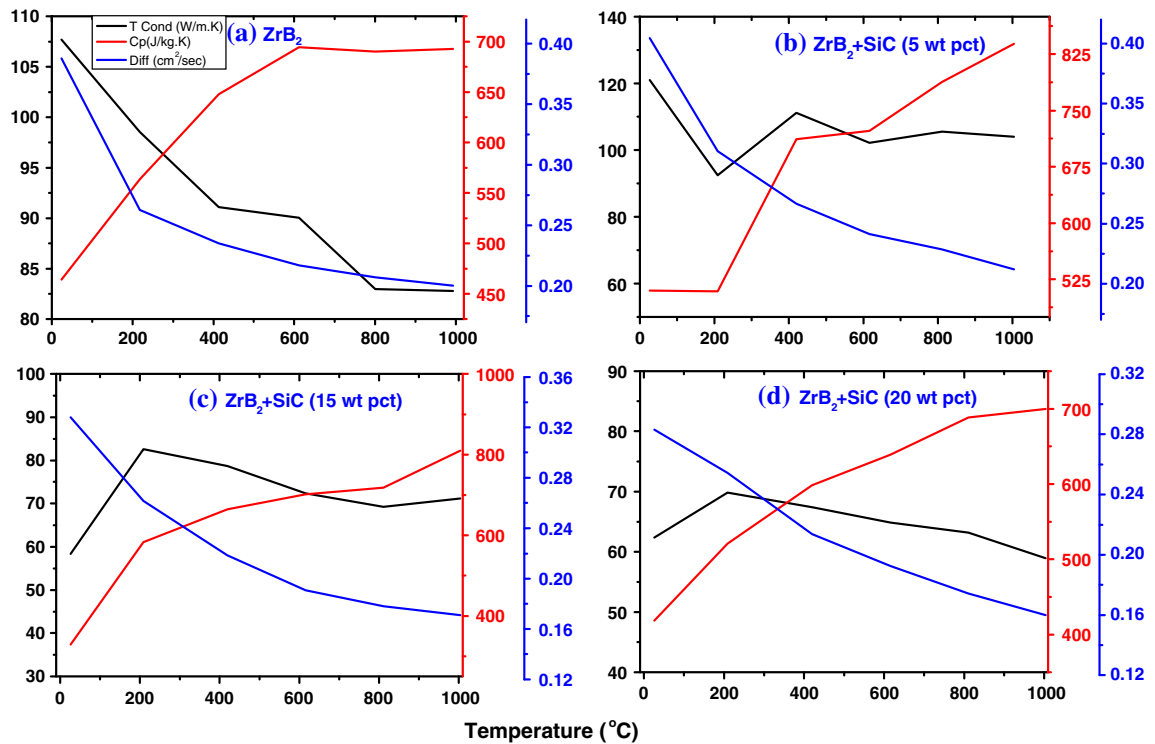
Fig. 7—Thermal properties of (*a*) monolithic ZrB$_2$, (*b*) ZrB$_2$-SiC (5 wt pct), (*c*) ZrB$_2$-SiC (15 wt pct), and (*d*) ZrB$_2$-SiC (20 wt pct) composites.

Table IV. Interfacial Resistance Values of Monolithic ZrB$_2$ and ZrB$_2$-SiC Composites Hot Pressed at 2473 K (2200 °C)/2 h

Compositions	Measured R_{int}^* (m^2 K W^{-1})
ZrB$_2$	3.893×10^{-8}
ZrB$_2$ + SiC (5 wt pct)	3.448×10^{-8}
ZrB$_2$ + SiC (10 wt pct)	5.631×10^{-8}
ZrB$_2$ + SiC (20 wt pct)	5.476×10^{-8}

data points in the λ^{-1} *vs* T (in K) plot can be fitted to a straight line correlating with Eq. [4][52]:

$$\lambda_{\text{poly}}^{-1} = aT + n_l/lR_{\text{int}}^*, \quad [4]$$

where *a,* the slope of the plot is constant and inherent to the phonon–phonon scattering within the grains, which is independent to grain size; n_l the number of grain boundaries in distance *l*; R_{int}^* the grain boundary thermal resistance for unit area.

IV. CONCLUSIONS

In this work, ZrB$_2$-SiC composites were prepared by hot pressing at 2473 K (2200 °C) for 2 hour soaking under 50 MPa pressure with varying amount of SiC (5 to 20 wt pct) and studied the effect of the SiC loading on bulk density, phase composition and microstructure, mechanical properties like hardness, fracture toughness, scratch resistance, wear resistance, and thermal conductivity of ZrB$_2$-SiC composites and compared with similar characteristics of monolithic ZrB$_2$. Addition of micron-sized SiC in ZrB$_2$ system showed better mechanical properties like Vickers hardness, fracture toughness, scratch resistance, and wear resistance. It was also observed that thermal conductivity of ZrB$_2$-SiC composite showed higher value at the addition of SiC (5 wt pct) and decreased slowly with increasing temperature than ZrB$_2$ monolithic especially between 873 K and 1273 K (600 °C and 1000 °C) that means the ZrB$_2$-SiC composites can withstand better thermal fluctuations at higher temperature. At higher loading of SiC

nanosized SiC in ZrB$_2$ matrix increased the thermal conductivity (~80 to 100 W/m K), and value was about twice as large as those of coarse SiC.[51] The dependency of thermal diffusivity on SiC loading is similar to that of thermal conductivity. The variations of specific heat of different specimens with temperature are also shown in Figure 7. The heat capacity of all ZrB$_2$-SiC composites is higher than monolithic ZrB$_2$, since the specific heat of pure material is in the following order C_p (SiC) > C_p (ZrB$_2$). At higher loading of SiC (>5 wt pct), the presence of more interfaces and porosity between ZrB$_2$ and SiC grains (Figures 4(c) through (d)) could form high interfacial thermal grain boundary resistance (or Kapitza resistance, R_{int}^*) and hence reduce the thermal conductivity with respect to monolithic ZrB$_2$.[19] An analysis of the Kapitza resistance of monolithic ZrB$_2$ and ZrB$_2$-SiC composites is listed in Table IV for better understanding of the above statement. The measurements are recorded from 373 K to 1273 K (100 °C to 1000 °C) temperature range, and the

(15 wt pct and above), interfacial thermal grain boundary resistance can play the key role and reduces the thermal conductivity of the composite.

ACKNOWLEDGMENTS

REFERENCES

1. J.K. Sonber and A.K. Suri: *Adv. Appl. Ceram.*, 2011, vol. 110, pp. 321–34.
2. S.-Q. Guo: *J. Euro. Ceram. Soc.*, 2009, vol. 29, pp. 995–1011.
3. F. Monteverde and A. Bellosi: *J. Electrochem. Soc.*, 2003, vol. 150, pp. B552–59.
4. E. Wuchina, E. Opila, M. Opeka, W. Fahrenholtz, and I. Talmy: *Electrochem. Soc. Interface*, 2007, vol. 16, pp. 30–36.
5. H.O. Pierson: *Handbook of Refractory Carbides and Nitrides*, Noyes Publications, Westwood, 1996, pp. 55–78.
6. W.G. Fahrenholtz, G.E. Hilmas, I.G. Talmy, and J.A. Zaykoski: *J. Am. Ceram. Soc.*, 2007, vol. 90, pp. 1347–64.
7. K. Upadhya, J.M. Yang, and W.P. Hoffmann: *Am. Ceram. Soc. Bull.*, 1997, vol. 76, pp. 51–56.
8. A. Paul, D.D. Jayaseelan, S. Venugopal, E. Z-Solvas, and J. Binner: *J. Am. Ceram. Soc Bull.*, 2012, vol. 91, pp. 22–29.
9. E. Sani, L. Mercatelli, D. Jafrancesco, J.L. Sans, and D. Sciti: *J. Eur. Opt. Soc.*, 7 (2012)12052 (5p).
10. C.-W. Li, Y.-M. Lin, M.-Fu. Wang, and C.A. Wang: *Front. Mater. Sci. China*, 2010, vol. 4, pp. 271–75.
11. A.K. Kuriakose and J.L. Margrave: *J. Electrochem. Soc.*, 1964, vol. 111, pp. 827–31.
12. M. Donohue, C. Carpenter, and N. Orlovskaya: *NATO Science for Peace and Security Series B: Physics and Biophysics, Boron rich chapter*, 2011, pp. 287–302.
13. L. Pienti, D. Sciti, L. Silvestroni, and S. Guicciardi: *Materials*, 2013, vol. 6, pp. 1980–93.
14. D. Sciti, L. Silvestroni, G. Saccone, and D. Alfano: *Mater. Chem. Phys.*, 2013, vol. 137, pp. 834–42.
15. F. Yang, X. Zhang, J. Han, and S. Du: *Mater. Des.*, 2008, vol. 29, pp. 1817–20.
16. S. Kim, J.M. Cha, S.M. Lee, Y. Sukoh, H. Kim, and B.K. Jang: *Ceram. Int.*, 2014, vol. 40, pp. 3477–83.
17. F. Monteverde: *Appl. Phys. A-Mater. Sci. Proc.*, 2006, vol. 82, pp. 329–37.
18. A. Rezaie, W.G. Fahrenholtz, and G.E. Hilmas: *J. Mater. Sci.*, 2007, vol. 42, pp. 2735–44.
19. J.W. Zimmermann, G.E. Hilmas, W.G. Fahrenholtz, R.B. Dinwiddie, W.D. Porter, and H. Wang: *J. Am. Ceram. Soc.*, 2008, vol. 91, pp. 1405–11.
20. D.D. Jayaseelan, E.Z. Solvas, P. Brown, and W.E. Lee: *J. Am. Ceram. Soc.*, 2012, vol. 95, pp. 1247–54.
21. M.M. Opeka, I.G. Talmy, and J.A. Zaykoski: *J. Mater. Sci.*, 2004, vol. 39, pp. 5887–909.
22. F. Monteverde and A. Bellosi: *Adv. Eng. Mater.*, 2004, vol. 6, pp. 331–36.
23. Z.Y. Pan, Y. Wang, X.W. Li, C. Wang, and Z.W. Zou: *J. Therm. Spray Tech.*, 2012, vol. 21, pp. 95–1009.
24. M.S. Datta, A.K. Bandyopadhyay, and B. Chaudhuri: *Bull. Mater. Sci.*, 2002, vol. 25, pp. 181–89.
25. S. Prochazka and R.M. Scanlan: *J. Am. Ceram. Soc.*, 1975, vol. 58, pp. 72–76.
26. M. Ikegami, S. Guo, and Y. Kagawa: *Ceram. Int.*, 2012, vol. 38 (1), pp. 769–74.
27. M.S. Asl and M.G. Kakroudi: *Ceram. Int.*, 2014, vol. 40, pp. 15273–81.
28. G.R. Anstis, P. Chantikul, B.R. Lawn, and D.B. Marshall: *J. Am. Ceram. Soc.*, 1981, vol. 64, pp. 533–38.
29. A. Iost and R. Bigot: *J. Mater. Sci.*, 1996, vol. 31, pp. 3573–77.
30. S. Chakraborty, D. Debnath, A.R. Mallick, and P.K. Das: *Int. J. Refrac. Met. Hard Mater.*, 2014, vol. 46, pp. 35–42.
31. J. Fang, H.M. Chan, and M.P. Harmer: *Mater. Sci. Eng., A*, 1995, vol. 195, pp. 163–67.
32. J.P. Singh, H. Baba, S. Hayashi, and A. Suzuki: *Proc. 21st Ann. Conf. Compos. Adv. Ceram. Mater. Struct.: A: Ceram. Eng. Sci. Proc.*, 2008, 18, Chapter 28.
33. Q. Liu, W. Han, X. Zhang, S. Wang, and J. Han: *Mater. Lett.*, 2009, vol. 63, pp. 1323–25.
34. W.M. Guo, Z.G. Yang, and G.J. Zhang: *Ceram. Int.*, 2013, vol. 39, pp. 7229–33.
35. C.B. Ponton and R.D. Rawlings: *Mater. Sci. Tech.*, 1989, vol. 5, pp. 865–72.
36. C.B. Ponton and R.D. Rawlings: *Mater. Sci. Tech.*, 1989, vol. 5, pp. 961–76.
37. J. Mukherjee, S. Chakraborty, S. Chakravarty, A. Ranjan, and P.K. Das: *Ceram. Int.*, 2014, vol. 40, pp. 6639–45.
38. D.C. Cranmer: *Tribo. Trans.*, 1988, vol. 31, pp. 164–73.
39. T.N. Ying, M.C. Shen, Y.S. Wang, and S.M. Hsu: *Tribo. Trans.*, 1997, vol. 40, pp. 685–93.
40. J.F. Archard: *J. Appl. Phy.*, 1953, vol. 24, pp. 981–88.
41. M. Gasch, S. Johnson, and J. Marschall: *J. Am. Ceram. Soc.*, 2008, vol. 91, pp. 1423–32.
42. W. Li, L. Li, T. Cheng, C. Zhang, and D. Fang: *Phys. Scr.*, 2012, vol 86, pp. 055402.
43. W. Tian and R. Yang: *Comp. Model. Eng. Sci.*, 2008, vol. 24, pp. 123–41.
44. G. Anirthan, A. Udaya Kumar, and M. Balsubramanian: *Ceram. Int.*, 2011, vol 37, pp. 423–26.
45. E. Z-Solvas, D.D. Jayaseelan, P.M. Brown, and W.E. Lee: *J. Eur. Ceram. Soc.*, 2013, vol. 33, pp. 3467–72.
46. M. Patel, B.V.V. Prasad, and V. Jayaram: *J. Eur. Ceram. Soc.*, 2013, vol. 33, pp. 615–1624.
47. J.W. Lawson, M.S. Daw, and C.W. Bauschlicher: *J. Appl. Phys.*, 2011, vol. 110, p. 083507-4.
48. G.A. Slack: *J. Phys. Chem. Solids*, 1973, vol. 34, pp. 321–35.
49. L. Zhang, D.A. Pejaković, J. Marschall, and M. Gasch: *J. Am. Ceram. Soc.*, 2011, vol. 94, pp. 2562–70.
50. M. Patel, V.V.B. Prasad, and V. Jayaram: *J. Eur. Ceram. Soc.*, 2013, vol. 33 (10), pp. 1615–24.
51. S. Kima, J.-M. Chae, S.-M. Lee, Y.-S. Oh, H.-T. Kim, and B.-K. Jang: *Ceram. Int.* 2014, vol 40, pp. 3477–83.
52. D.S. Smith, S. Fayette, S. Grandjean, C. Martin, R. Telle, and T. Tonnessen: *J. Am. Ceram. Soc.*, 2003, vol. 86, pp. 105–11.